ANALYTICAL BIOCHEMISTRY 231, 92–98 (1995)

Determination of Local Refractive Index for Protein and Virus Crystals in Solution by Mach–Zehnder Interferometry

Tammy Cole,* Alan Kathman,* Stan Koszelak,† and Alex McPherson†,[1]

*Teledyne Brown Engineering, Huntsville, Alabama; and †Department of Biochemistry, University of California at Riverside, Riverside, California 92521

Received May 4, 1995

To establish the importance of, and quantitatively evaluate, the macromolecular concentration gradients in the neighborhood of growing protein, virus, and nucleic acid crystals, a convenient, accurate, and nonintrusive method has been devised. This approach should prove particularly relevant in the rigorous comparison of crystals grown in a conventional laboratory setting with those grown in a microgravity environment. The method is based on precise determination of the local refractive index using Mach–Zehnder interferometry. Presented here are data for five protein and three virus systems. From data for these and other systems, optical monitoring experiments to measure local growth conditions and growth kinetics in liquid–liquid diffusion, batch, and vapor diffusion crystal growth experiments can be designed.

Further exploitation of the X-ray diffraction technique to provide a precise structural basis for molecular biology now depends crucially on an understanding and mastery of macromolecular crystallization (1–3). This in turn requires that quantitative methods be developed for the investigation and characterization of the crystallization process (4). Of substantial importance in the investigation of macromolecular crystallization is an accurate characterization of the fluid environment of growing crystals, particularly the protein, or nutrient, concentration. By delineating the effective concentration gradients in these regions, the influence of transport processes on crystal growth can be evaluated. In addition, an important technique used to promote macromolecular crystallization is the direct liquid–liquid diffusion approach (1,5). To accurately describe the kinetics of experiments using liquid–liquid diffusion, it is useful to be able to monitor, and particularly to quantitate, the progress of the diffusion process. The method described here is well suited for that purpose.

To quantitate diffusion fields at liquid–liquid interfaces and around growing crystals, Mach–Zehnder interferometry (6) was employed. This approach has the advantages of simplicity, economy, and an extensive history of application in evaluating density changes in transparent media. Here, we show that for five different protein systems, and three different viruses, the method can be used to precisely monitor concentrations in a rapid, convenient, and nonintrusive manner.

MATERIALS AND METHODS

Interferometry involves the division of a beam of light into two separate beams which are subsequently recombined. In the absence of any path differences, the two beams will combine with uniform constructive interference (no visible effects). Introducing a linear path difference or tilt between the two beams will result in the appearance of straight interference fringes. These can often be used as a reference condition. If a sample is placed in one of the two beams such that the varying concentration and density of a dissolved specie produces a change in refractive index at some point in the field of the beam, the resultant optical path length differences will produce perturbations in the fringe structure. The degree of deviation of the fringe pattern from the reference condition can then be directly correlated to a change in the refractive index, and ultimately, to the relative concentration of the macromolecule.

[1] To whom correspondence should be addressed. Fax: (909) 787-3790.

0003-2697/95 $12.00

The optical path length (OPL)[2] of a collimated laser beam through a growth cell can be represented by

$$\mathrm{OPL} = \int_L n(x,y,z)\, dz,$$

where $n(x,y,z)$ represents the index of refraction throughout a given volume of fluid and L is the physical path length through the fluid in the z direction. Interfering this two-dimensional OPL map with a planar reference beam will produce a set of fringes or interferogram. Because each pair of light/dark fringes represent an optical path difference of one wavelength (λ) the relative OPL can also be calculated to a fraction of a wavelength.

From this relationship, the pitch and position of fringes in an interferogram of the test cell can be directly related to the transverse index gradient within that volume. Because, for a known temperature, the index of refraction can be directly related to the concentration of the protein or virus solution, the change in concentration can be determined from experimentally measured parameters. If the index of refraction is known for any point in the sample, then the change in index can be used to calculate a quantitative value for the index at any other location in the fluid.

In the experiments analyzed here, the protein or virus solution was simply layered atop a second buffer solution lacking the macromolecule. Once diffusion initiates between two liquids, the index of the fluid in the vicinity of the diffusion layer continually varies. Upon approach to the initial interface between the two fluids, the concentration gradient increases to a maximum. This produces a change in the phase of the transmitted light, which causes the fringes to curve. The greater the concentration gradient the greater the fringe curvature.

For an initial, qualitative evaluation of the experimental arrangement a solution of NaCl was layered upon distilled water. The Mach–Zehnder interferometer was configured to exhibit vertical fringes in the absence of a concentration gradient. These vertical fringes act as a "carrier frequency" to prevent fringe ambiguity in the measurement. They are perpendicular to the gradients to be measured and therefore do not compromise the accuracy of the experiment. As the sample was translated vertically through the field of view and different points within the diffusion layer observed, the sequence of images seen in Fig. 1 were obtained. Apparent in these photographs is the dramatic bending of the fringes toward the center of the diffusion layer contrasted with their relatively straight appearance in the regions of pure solution.

Figure 2 illustrates the change in index for given increments vertically through the test cell. The relative amount of fringe bending was measured by the number of fringes crossing a stationary vertical line. In areas containing pure solution, fringes were straight with no horizontal component; no index gradients were present. Upon approach to the initial diffusion boundary, greater numbers of horizontal fringes become evident, indicating more severe gradients in that region of the fluid. As expected, the change in index over a given vertical path increases dramatically upon approach to the initial liquid–liquid interface.

A schematic of the Mach–Zehnder interferometer is shown in Fig. 3. A 10 mW helium–neon laser (Uni-Phase) was directed through a spatial filter and collimation lens toward a 50/50 cubic beamsplitter. The two emerging beams formed the legs of the interferometer and were redirected toward a second 50/50 beamsplitter which acted as a beam combiner. The sample was positioned in the path of one leg of the interferometer using a series of translation stages. The combined beam exiting one side of the beam combiner was directed through 80 and 800-mm focal length lenses positioned so as to produce a 10× magnification on the face of the CCD camera (Sony, XC-75). (The part of the beam passing through the other side of the beam combiner was used for schlieren imaging.) The output from the camera was directed to a 386 PC equipped with a frame grabber. A super-VHS time-lapse video cassette recorder was also interfaced with the system to allow video recording of the images. Neutral density filters were placed in front of the camera to avoid saturation of the CCD.

The proteins studied in these experiments were hemoglobin, pepsin, ribonuclease B, pepsinogen, and lysozyme. All were purchased from Sigma Biochemical Co. (St. Louis, MO) and dissolved in distilled water. No further purification was performed. The viruses employed here were satellite tobacco mosaic virus (STMV) a $T = 1$ spherical virus, turnip yellow mosaic virus (TYMV), and cucumber mosaic virus (CMV), both $T = 3$ spherical viruses. The virus samples were all isolated and purified by the authors according to published procedures [STMV (7), TYMV (8), CMV (9)]. All of the virus samples were recrystallized at least once prior to use.

Experimental Procedure for the Interferometry Measurements

The samples were contained in quartz cuvettes. A liquid–liquid diffusion layer was formed by layering a given volume of distilled water on top of an equal volume of protein or virus solution. In order to ensure

[2] Abbreviations used: OPL, optical path length; STMV, satellite tobacco mosaic virus; TYMV, turnip yellow mosaic virus; CMV, cucumber mosaic virus.

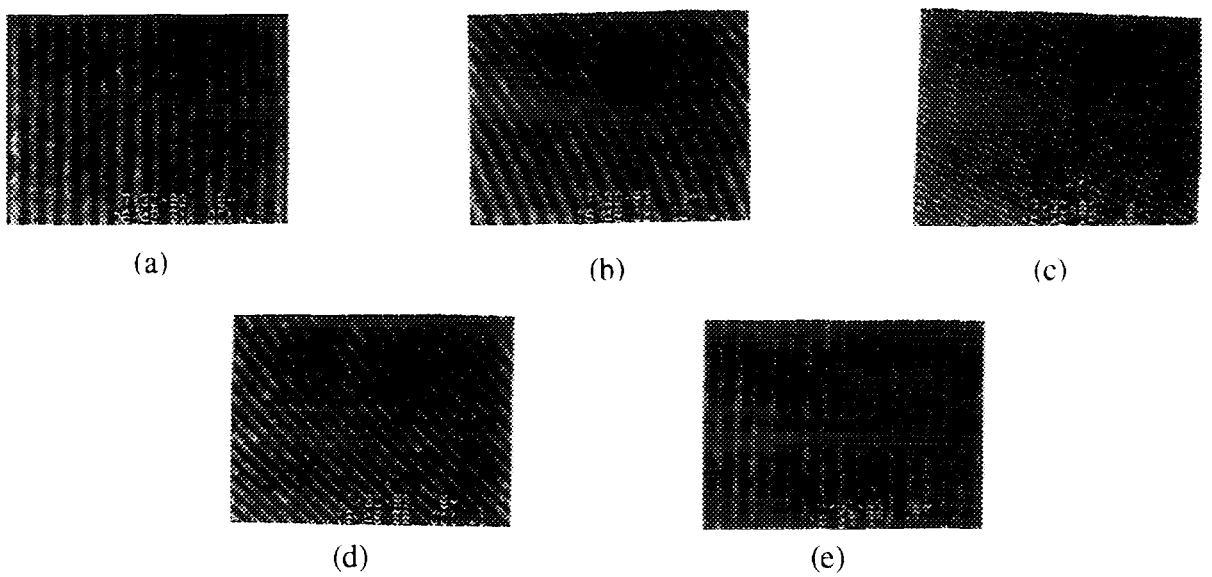

FIG. 1. Fringe structures at selected points in the liquid–liquid diffusion experiment: (a) in unmixed 18.9% aqueous NaCl, (b) entering the mixing layer, (c) nearing the initial diffusion point, (d) leaving the mixing layer and approaching the distilled water, (e) in the unmixed distilled water.

a clean boundary between the two fluids, mixing was minimized by pipetting the water down a glass fiber suspended over the cuvette. The fiber touched the side of the cuvette just above the level of the fluid. This configuration allowed the water to be slowly added at one location, and it focused most of the turbulent mixing near the edge of the container, away from the central region under study (See Fig. 4). The layering process was interferometrically observed in real time to ensure that mixing was minimal in the test region. In most cases the fluids layered quite well, but in some cases measurement had to be delayed because the fringes in the area of the initial diffusion point showed a sharp discontinuity and were too dense to be resolved by the system.

During the course of determining a protein's test matrix, the concentration was sequentially diluted. As each interferometry test was completed, equal volumes of water and the protein solution were pipetted into an Eppendorf tube and mixed. This dilution formed the next concentration for study. All protein samples were centrifuged for approximately 3 min prior to the test.

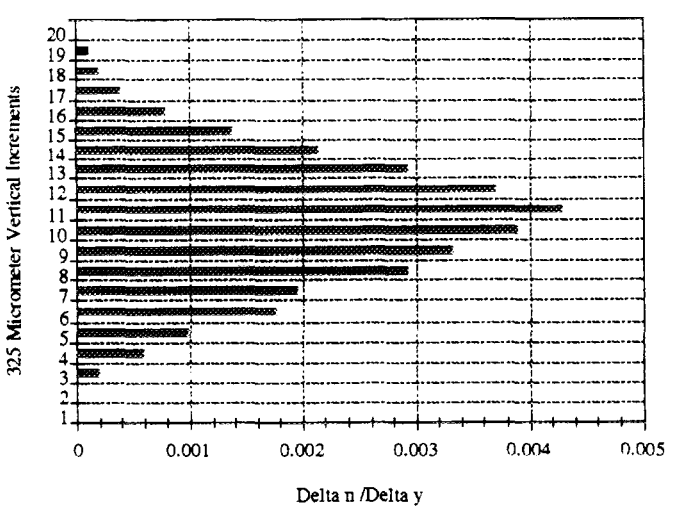

FIG. 2. Measured index of refraction gradients present in a vertical cross-section of the diffusion layer created by distilled water layered onto 6.5% aqueous NaCl.

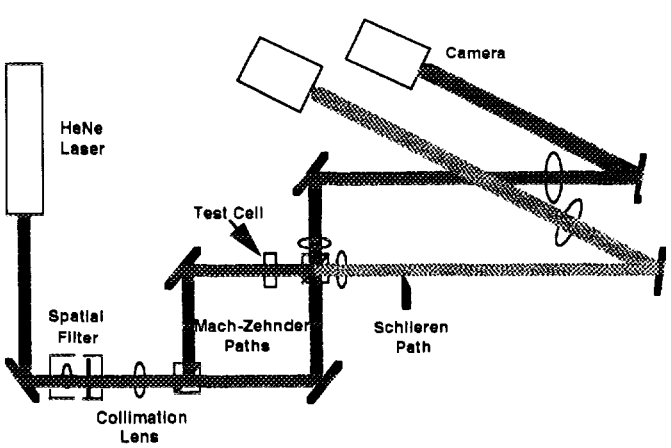

FIG. 3. Schematic of the Mach–Zehnder system.

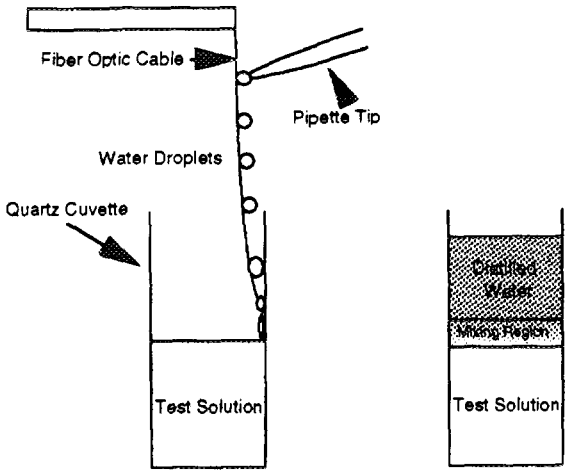

FIG. 4. Procedure for establishing a liquid–liquid diffusion layer and the resulting regions.

This process generally resulted in slight amounts of residue which were discarded.

Characterization of the Interferometer System

Prior to carrying out the protein and virus experiments, efforts were made to characterize the interferometer using known concentrations of NaCl in water. The data from these experiments were then plotted with accepted values for the index of refraction (10). The results are shown in Fig. 5. These standard concentrations were prepared in our laboratory. Estimates of error were made and are shown as error bars on the graph. The error on the mass measurements was ±0.01 g. The error on the volume measurements was ±0.1 ml. This uncertainty in volume was largely responsible for the concentration error bars. As seen in Fig. 5, experimental points agreed with accepted values within the error of measurement. This graph estimates the error in the index of refraction measurements made by this technique to be approximately ±0.001.

Verification of Concentrations

Concentrations of proteins and viruses were confirmed using a spectrophotometer (Perkin–Elmer Lambda 3B). Samples taken from the initial and final concentrations of the macromolecules were diluted to ensure a linear relationship between concentration and absorption. The spectrophotometer was used to measure absorption at 280 nm, which was then converted to concentration using the standard correction coefficients for the proteins. The beginning and ending concentrations were adjusted using the results of the absorption tests. The test matrix of concentrations was then adjusted accordingly.

Since correction coefficients for the viruses have not yet been determined, we obtained concentration versus absorption plots for both STMV and TYMV. (Insufficient CMV was available to perform this analysis.) The data were plotted versus concentration and a best-fit line was calculated. The equation of this line was then used to adjust the concentration values for the virus samples. Although this did not correct for error in the initial concentration, it did assist in correcting for error introduced through the dilution process.

RESULTS

Fringe structures in both the protein and the virus samples were similar to those found in the NaCl experiments. There was sharp bending as the fringes approached the initial boundary layer between the two fluids and, as previously observed in the characterization studies, the fringes slowly straightened over time until the fluids reached homogeneity. The fringes then formed straight, continuous fringes throughout the sample volume.

Index of Refraction Measurements for Proteins

Figures 6a–6e show index of refraction versus corrected concentrations for each of the proteins, and Fig. 6f is a compilation of these graphs. Equations of best-fit lines are included with appropriate graphs. By far the largest fractional difference between expected and measured final concentration occurred with hemoglobin, where there was a 40% differences. This large difference may be attributable to the relatively large quantities of amorphous material that separated from the hemoglobin samples during centrifugation prior to index measurements. Other protein concentrations varied less. There was a 9.41% difference in the case of pepsin, a 4.23% difference in the case of ribonuclease B, a 2.38% differences for pepsinogen, and a 1.86% difference for lysozyme.

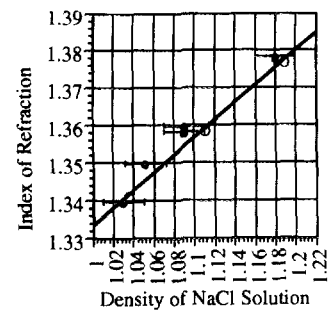

FIG. 5. Data taken to characterize the Mach–Zehnder system. Standard values are represented by open circles and experiment data are represented by filled circles. Error bars are included for experimental data.

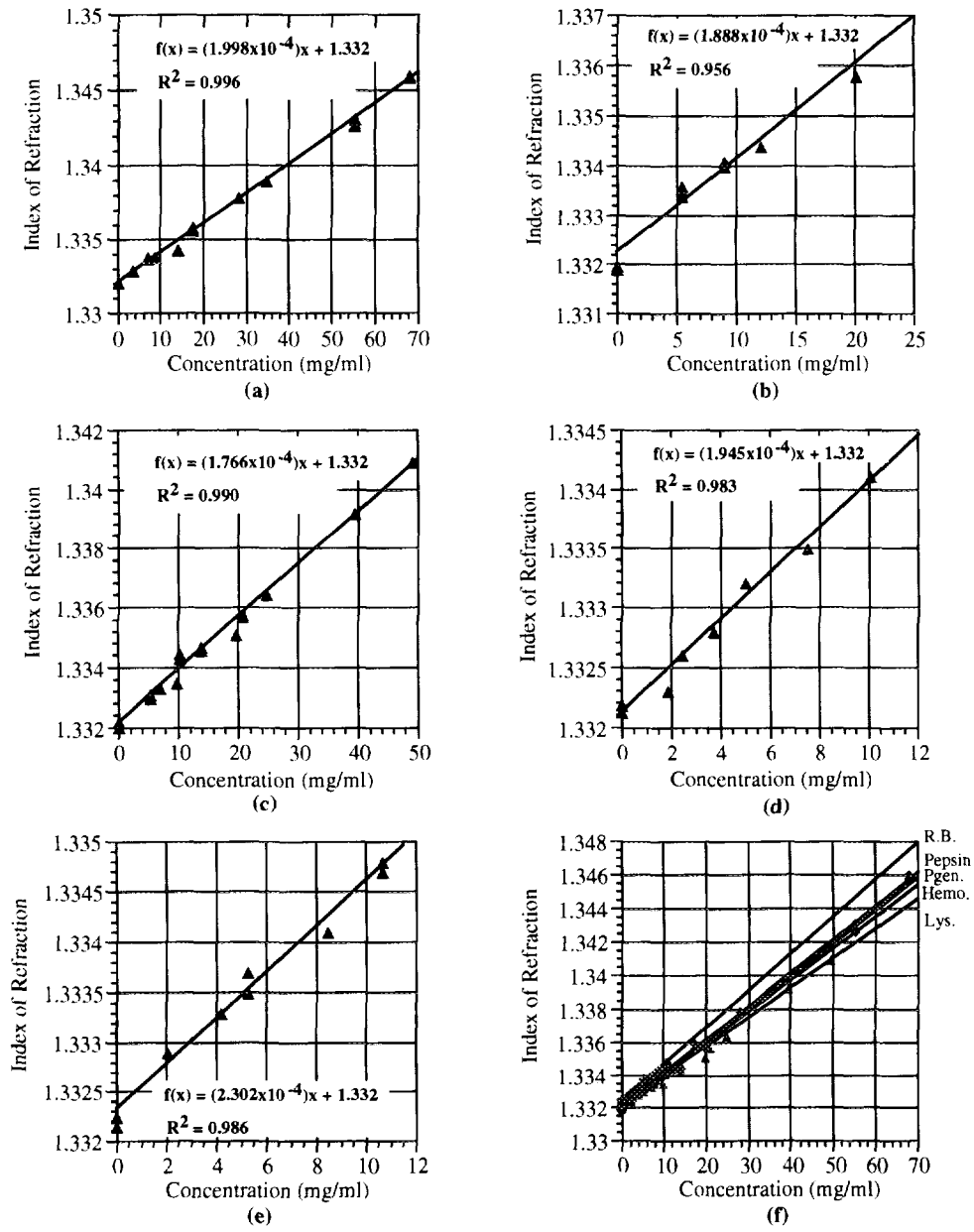

FIG. 6. Index of refraction verses concentration data for the selected proteins: (a) pepsin, (b) hemoglobin, (c) lysozyme, (d) pepsinogen, (e) ribonuclease B. A compilation of protein data is shown in (f). All graphs have been corrected for errors produced during dilution.

All of the graphs shown in Fig. 6 display a strong linear dependence between index of refraction and concentration. Since we were dealing with relatively low protein concentrations, this was not surprising. Such a linear dependence would be expected for concentrations below the saturation region. The vast majority of the data points fall on the best-fit line within predicted experimental error.

Although there are slight differences in the index relationships for each of the proteins, Fig. 6f illustrates that the indices for all proteins are fairly similar in magnitude. This is, again, not surprising, since the proteins are quite similar in chemical composition and physical size.

Index of Refraction Measurements for Viruses

Figure 7 shows absorption versus concentration for TYMV and STMV, with TYMV showing particularly good linearity. The best-fit line from this graph was

used to calculate dilution errors, and the data were corrected as described above. The resulting index versus concentration is shown in Fig. 8a along with the equation of the best-fit line.

Absorption versus concentration for STMV is shown in Fig. 7b. Results in this case were not as straightforward as with TYMV. The graph shows both the best linear and power fits. The data did not provide a particularly good linear fit. Furthermore, in the absence of STMV, the absorption should have been zero and the line representing absorption should have passed through the origin, as it does for TYMV. The equation of the best-fit line, however, does not produce an absorption of zero in the absence of STMV. Forcing the data through zero produces the curve shown. The shape of this curve suggests that there may be some saturation of the transition responsible for the absorption. Because these findings were inconclusive, these data were not used to correct for dilutional errors in the index measurements.

Figure 8 shows the index of refraction for each of the virus samples and Fig. 8d shows the combined graphs for TYMV that have been corrected for dilutional errors using the absorption versus concentration curves presented above. The STMV and CMV graphs were not corrected.

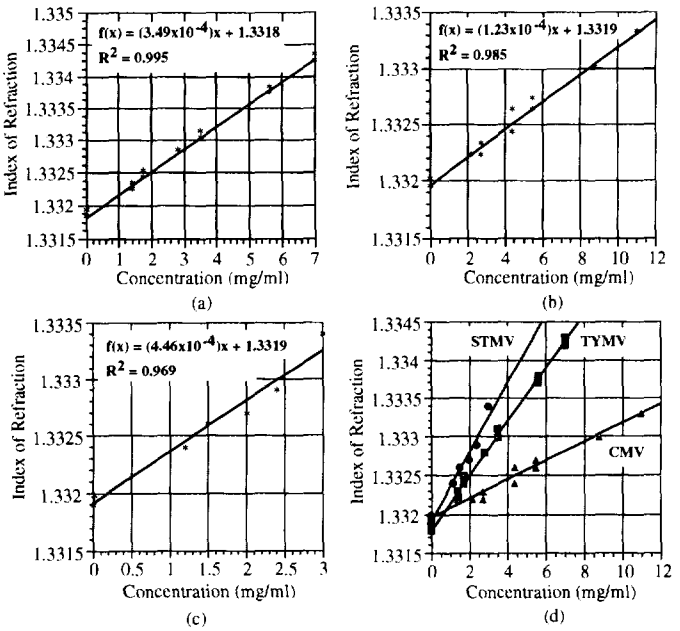

FIG. 8. Index of refraction versus concentration data for the selected viruses: (a) TYMV at 23.7 ± 0.4°C, (b) STMV at 22.6 ± 0.4°C, (c) CMV at 22.4 ± 0.3°C. The TYMV graph has been corrected for errors produced during dilution. The equations represent the best-fit lines shown in the graphs. A compilation of virus data is shown in (d).

CONCLUSIONS

The experiments presented here show that a simple Mach–Zehnder interferometry technique can be used to map macromolecular concentration fields within a small volume of fluid in a precise and noninvasive manner. The approach appears promising for the purpose of quantitating concentration gradients in the neighborhoods of growing protein, virus, or nucleic acid crystals. Using this technique, the variations in the refractive index of five different proteins and three different virus samples were measured. All proteins and viruses exhibited an expected linear relationship between index of refraction and concentration within the ranges studied. It was also found that the relative values of index of refraction did not vary substantially among the different samples.

We would like to note that the conventional Mach–Zehnder interferometric method used here could be made substantially more sensitive and could provide far higher resolution of concentration, by introducing phase shift interferometric techniques. We feel that at least a 20-fold improvement may be readily achieved in this way. A phase shift Mach–Zehnder interferometer is now under construction to demonstrate this hypothesis.

Currently there are a number of investigations using a variety of space vehicles to study the effects of gravity on the processes that define macromolecular crystal growth (11–14). A principal objective of this research is to obtain a clear representation of the local supersaturation and the concentrations of nutrients and impurities in the immediate environment of growing crystals. This must be done *in situ* and in a completely nonintrusive manner. The method described here fulfills those objectives and does so within the constraints of the experimental systems.

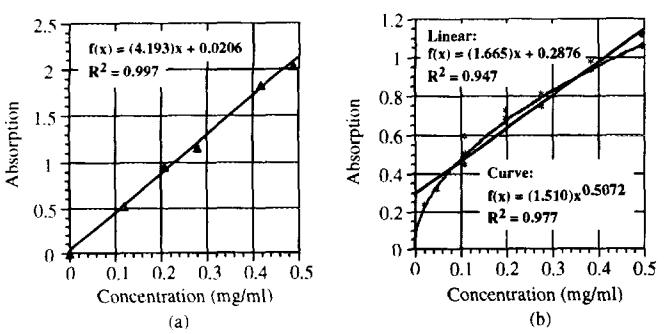

FIG. 7. Absorption curves for (a) TYMV and (b) STMV. Equations shown are for the best-fit lines/curves shown in the graphs.

ACKNOWLEDGMENTS

This research was supported by a grant from the National Aeronautics and Space Administration (NASA). The authors wish to

thank those NASA and ESA personnel who contributed to the success of these experiments.

REFERENCES

1. McPherson, A. (1982) Preparation and Analysis of Protein Crystals, Wiley, New York.
2. Ducruix, A., and Giege, R. (1992) Crystallization of Nucleic Acids and Proteins: A Practical Approach, IRL Press, Oxford.
3. Carter, C. W. (1990) Protein and Nucleic Acid Crystallization Methods: A Companion to Methods in Enzymology, Academic Press, New York.
4. Wells, M., Cole, T., Kathman, A., Koszelak, S., and McPherson, A. (1994) *in* AIAA Proceedings, Vol. 94-4552.
5. Salemme, F. R. (1972) *Arch. Biochem. Biophys.* **151,** 533–537.
6. Kathman, A., Cole, T., Wells, M., Jenkins, G., Koszelak, S., and McPherson, A. (1994) *in* SPIE Proceedings, pp. 2214–2236.
7. Koszelak, S., Dodds, J. A., and McPherson, A. (1989) *J. Mol. Biol.* **209,** 323–325.
8. Canady, M. A., Day, J., and McPherson, A. (1995) *Proteins* **21,** 78–81.
9. Kaper, J. M., and Waterworth, H. E. (1981) Handbook of Plant Virus Infections and Comparative Diagnosis, (Kurstak, E., Ed). pp. 259–322, Elsevier, North-Holland Biomedical, Amsterdam.
10. Weast, R., Astle, M., and Beyer, W. (Eds.) (1983) Handbook of Chemistry and Physics, CRC Press, Boca Raton, FL.
11. DeLucas, L. J., Smith, C. D., Smith, H. W., Senagdi, V. K., Senadhi, S. E., Ealick, S. E., Bugg, C. E. Carter, D. C., Snyder, R. S., Weber, P. C., Salemme, F. R., Ohlendorf, D. H., Einspahr, H. M., Clancy, L., Navia, M. A., Mckeever, B. M., Nagabhushan, T. L., Nelson, G., Babu, Y. S., McPherson, A., Koszelak, S., Stammers, D., Powell, K., and Darby, G. (1989) *Science* **246,** 651–654.
12. Day, J., and McPherson, A. (1992) *Protein Sci.* **1,** 254–268.
13. McPherson, A. (1993) *J. Phys. D. Appl. Phys.* **26,** B104–B112.
14. DeLucas, L. J., and Bugg, C. E. (1987) *Trends Biotechnol.* **5,** 188–192.